Panchromatic Thin Perovskite Solar Cells with Broadband Plasmonic Absorption Enhancement and Efficient Light Scattering Management by Au@Ag Core-Shell Nanocuboids

Nianqing Fu[a,b#], Zhi Yong Bao[b#], Yong-Liang Zhang[b], Guoge Zhang[a], Shanming Ke[c], Peng Lin[c], Jiyan Dai[b], Haitao Huang[b]*, and Dang Yuan Lei[b]*

(# Nianqing Fu and Zhi Yong Bao contributed equally to this work.)

[a]School of Materials Science and Engineering, South China University of Technology, Guangzhou 510640, China.

[b]Department of Applied Physics, The Hong Kong Polytechnic University, Hong Kong, China.

[c]Guangdong Research Center for Interfacial Engineering of Functional Materials, College of Materials Science and Engineering, Shenzhen University, Shenzhen, 518060, China.

*Corresponding author:

Haitao Huang (H. Huang), E-mail: aphhuang@polyu.edu.hk,

Dangyuan Lei (D. Lei), E-mail: dylei@polyu.edu.hk

Abstract

Enhancing the low-energy sunlight harvesting is of great importance for improving the efficiency of organic-inorganic halide perovskite solar cells (PSCs) but still remains a big challenge. Herein, we propose an improved light harvesting and management strategy by using rationally-designed Au@Ag core-shell nanocuboids as plasmonic inclusions, aiming at achieving panchromatic thin PSCs. Compared to conventional metal nanostructures with a single narrow plasmon resonance band, the Au@Ag nanocuboids exhibit multiple broader and stronger plasmon resonances that can be tuned by adjusting structural dimensions to spectrally match the absorption band of the perovskite, particularly in its weak absorption region. By carefully tailoring the location of the Au@Ag nanocuboids in the electrodes, both plasmonic near-field enhancement and increased light-scattering effects can be fully exploited to boost up the performance of the PSCs. As a result, the hybrid devices demonstrate high photon-to-electron conversion efficiency (IPCE) over the entire visible range, with a remarkable IPCE enhancement (ΔIPCE/IPCE) of 20-60% in the range of 550-750 nm, compared with pristine devices. This also leads to an average power conversion efficiency (PCE) of 17.83% for the optimized Au@Ag incorporated cells, with a champion PCE of 18.31% recorded for the best plasmonic PSC, corresponding to a PCE enhancement of 20.8%.

Keywords: perovskite solar cells; plasmonic enhancement; core-shell nanocuboids; broadband light harvesting; light management

1. Introduction

In the past decades, developing highly efficient yet inexpensive solar cells has been of supreme importance for fossil fuel preservation and environment protection. Among the emerging solar cell technologies, perovskite solar cells (PSCs) have attracted increasing attention in recent years due to their simple fabrication process, low-cost and high power conversion efficiency (PCE) [1-12]. Recently, PCE exceeding 22% has been achieved in perovskite solar cells [10]. However, it is still far from their theoretical limit, leaving rooms for improvement. One of the most effective approaches to further boost the efficiency of PSC is to increase the light harvesting efficiency [3,6], apart from improving the charge collection efficiency. In general, $CH_3NH_3PbI_{3-x}Cl_x$ based PSCs can harvest over 80% of the input high-energy illumination of 400-600 nm, but it fails to absorb the low-energy sunlight (λ_{Lo}) of 600-800 nm as effectively as it does in the high-energy zone (λ_{Hi}) due to the relatively poor extinction in the λ_{Lo} zone [6,13-15]. Actually, it is a hard task to achieve high incident photon-to-electron conversion efficiencies (IPCEs) at both λ_{Hi} and λ_{Lo} zones (Table S1, Supporting Information) [16-21], since a balanced high IPCE among the whole investigated wavelength range requires a precise control and optimization of the thickness, morphology, composition, traps, interface and grains of a relatively thick perovskite film ($\sim$ 400 nm) to yield a balanced high light harvesting and low charge recombination [16,18,20-25]. Moreover, this problem becomes more serious for semitransparent cells for building, because a thin perovskite layer ($\sim$250 nm) is usually required to keep semitransparency of the device [25-27]. This indicates that the effective utilization of the λ_{Lo} sunlight is a necessary approach to further promote the cell efficiency, which still remains a big challenge [6,16,25]. In this regard, developing a general, simple yet effective approach for a general researcher to realize broadband light harvesting and balanced high IPCE is highly desired for making panchromatic solar cells.

Extending the absorption edge of photoactive materials is a viable strategy to improve the light harvesting efficiency and maximizing the performance of various types of solar cells and other solar devices [28-33]. The well-known localized surface plasmon resonance (LSPR) of noble metallic nanoparticles (NPs) has been employed to enhance cell efficiency, by taking advantages of the LSPR induced synergistic effect of plasmonic enhancement in light absorption [29-34], increased light trapping/scattering [35,36], and direct resonant energy transfer [37-39]. To date, plasmonic NPs made of Au and/or Ag have been intensively studied for a plethora of applications in various kinds of solar cells, such as dye-sensitized solar cells (DSSCs) [29,30,39], organic photovoltaics (OPVs) and PSCs [35-38,40]. In the DSSC and OPV cases, the improvement in device efficiency is mainly due to the contribution of increased light harvesting by plasmonic NPs [29,30,35,36]. Unfortunately, such enhancement mechanism has not been observed in the plasmonic NP incorporated PSCs to date [38,41,42]. Most of the previous studies exploited spherical Ag, Au or Ag/Au@metal oxide NPs to boost the efficiency of solar cells [36-38,40,41]. Those Ag or Au nanospheres usually exhibit narrow plasmonic excitation bands (less than 100 nm in bandwidth) centered at 380 and 530 nm [36,37,41,42], which overlap with the strong extinction zone of the organic-inorganic metal halide perovskites ($CH_3NH_3PbI_3$, etc.). For example, Yuan et al. has recently revealed that the dominate contribution to the enhanced performance of plasmonic PSCs is the hot electron injection from Au NPs to TiO_x rather than plasmon-induced absorption enhancement [38]. This is simply because the plasmonic enhancement effect becomes less effective or nonexistent in the zone where the original absorption of the photoactive layer is already very significant [43]. This also explains why the conventional Ag or Au nanospheres can dramatically increase the light harvesting efficiency of DSSCs and OPVs but perform poorly in PSCs, that is, the extinction ability of common photoactive materials in DSSCs and OPVs is relatively lower than that in metal halide perovskites [43]. In this regard, using the conventional spherical plasmonic NPs to improve the light absorption of PSCs is usually

4

ineffective. The key to boosting the light collection capability and improving the efficiency of plasmonic NP incorporated PSCs lies in the broadening of the solar absorbing spectrum, especially in the λ_{Lo} region. To achieve this goal, novel plasmonic nanostructures that sustain broadband and tunable LSPR excitations are of paramount importance, yet seldom used in PSCs thus far.

The LSPR band of a metal NP depends on its shape, size and composition [44-48]. For example, a rod-like Au nanostructure generally exhibits two geometry-dependent LSPR bands due to the geometry anisotropy in the transverse and longitudinal directions, thus providing an additional degree of freedom, in comparison with a nanosphere, to alter its plasmonic extinction band by manipulating the aspect ratio [44,47]. Moreover, plasmon hybridization in a metal core-shell nanoparticle produces new plasmonic resonance bands such as subradiant and superradiant modes, higher-order resonances, and Fano resonances etc [49,50]. In this study, we successfully designed and synthesized a series of Au@Ag core-shell nanocuboids by a wet chemistry method [46]. The prepared nanocuboids have four broadened, tunable and intense plasmon resonance bands spanning the whole spectral range of 300-800 nm. By incorporating the Au@Ag nanocuboids with optimized dimensions in the sophisticated PSCs with well-prepared thin electrodes, the LSPR effects including plasmonic absorption enhancement and light scattering management can be fully exploited, leading to a synergistic enhancement in the performance of the plasmonic PSCs. The excellent plasmonic properties of the Au@Ag nanocuboids yielded a champion PCE of 18.31% and an average PCE of 17.83% (measured over 30 devices) for the hybrid PSCs, corresponding to 20.8% and 17.6% enhancement compared with pristine devices, respectively.

2. Experimental Section

2.1 Materials

Titanium (IV) isopropoxide (97%, TTIP), acetic acid, methylamine (40% in methanol), hydriodic acid (57 wt% in water), diethyl ether, hydrogen tetrachloroaurate (III) hydrate ($HAuCl_4 \cdot 4H_2O$), cetyltrimethylammonium bromide (CTAB), cetyltrimethyl-ammonium chloride (CTAC), silver nitrate ($AgNO_3$), ascorbic acid (AA), sodium borohydride, lead (II) Chloride ($PbCl_2$, 99.99%), and N,N-Dimethylformamide (DMF, 99.9%) were obtained from Sigma-Aldrich. The methylammonium iodide (CH_3NH_3I) was obtained from Dyesol. All chemicals were used as received without further purification. Ultrapure water was used for all experiments.

2.2 Syntheses of Au nanorods and Au@Ag nanocuboids

Au nanorods were synthesized by using a seed-mediated method [46]. Seed solution was synthesized by adding 0.6 mL of an ice-cold $NaBH_4$ (10 mM) solution into 10 mL of $HAuCl_4$ (0.25 mM) and CTAB (0.1 M) solution under vigorous stirring at room temperature. The color of the seed solution changed from yellow to brown. Growth solution was prepared by mixing 5 mL of $HAuCl_4$ (10 mM), 95 mL of CTAB (0.1 M), 1 mL of $AgNO_3$ (10 mM) and 0.55 mL of AA (0.1 M), consecutively. The solution was homogenized by gentle stirring. Then 0.12 mL of freshly prepared seed solution was added to the colorless solution and kept undisturbed in dark for 24 h. Prior to use, the Au nanorods solution was centrifuged twice at 8000 rpm for 10 min to remove excess CTAB and finally re-dispersed in DI water.

The Au@Ag core-shell nanocuboids were prepared according to a reported procedure with appropriate modifications [44,45]. Specifically, to coat the Au nanorods with Ag shells of varied thickness, 6 mL of the Au NRs solution were centrifuged and re-dispersed into an aqueous CTAC solution (0.08 M) at the same volume. Then, 1.2, 1.8, 2.0 and 2.4 mL of $AgNO_3$ (0.01 M) were subsequently added into four Au nanorods solutions of 6 mL, followed

by respective addition of 0.6, 0.9, 1.0 and 1.2 mL ascorbic acid solutions (0.1 M). The resultant solutions were kept in an isothermal oven at 65 °C for 4.5 h.

2.3 TiO₂ paste preparation

Organic-free anatase TiO_2 nanoparticle colloid with solid content of 3.5% was synthesized according to our previous work [51]. The AuNRs and Au@Ag nanocuboids were washed by DI water and collected by 8000 rpm centrifugation for five times to remove residual CTAB before adding into the TiO_2 paste. Appropriate amount of AuNRs or Au@Ag was dispersed in the TiO_2 paste by magnetic stirring and ultrasonication.

2.4 Electrodes and device fabrication

TiO_2 electrodes for mesoscopic perovskite solar cells were fabricated according to our previous work with modification [51]. Prior to deposition of the Au@Ag nanocuboids on the mesoscopic TiO_2 film, a ~30 nm compact TiO_2 layer was deposited on the patterned and well-cleaned FTO glass substrates [4]. For the mesoscopic TiO_2 film, TiO_2 pastes with/without AuNRs or Au@Ag were spin-coated at 2000 rpm for 50 s. For the coating of the plasmonic NP layer, the Au nanorods or Au@Ag aqueous solutions with various concentration (*e.g.* 1×10^{-10}, 2×10^{-10}, 4×10^{-10} M, Au based) were spread by spin-coating at 1000 rpm for 50 s. Four kinds of electrode configurations, namely Au@Ag below (#1), on the top of (#2), embedded in (#3), and embedded in and also on the top of (#4) the mesoscopic TiO_2 layer, were constructed by a layer-by-layer deposition process. After the coating of each layer, the electrodes were dried at 100 °C for 10 min. The thickness of the mesoporous TiO_2 film was controlled to be around 200 nm. After drying in air, all TiO_2 electrodes were carefully washed by an aqueous solution containing 2% ammonia (NH₄OH). Then, the electrodes were dipped into an isopropanol solution with 1 mM TTIP for a thin (around 2-3 nm) TiO_2 coating. After the film being dried in the air, a solution of 30 mM Li-TFSI (lithium bis-(trifluoromethylsulfonyl) imide salt) in acetonitrile was spin-coated on the TiO_2 film at 3000

rpm for 30 s to form the Li-doping of mesoporous TiO_2 film [52]. The dried TiO_2 electrodes were subjected to a fast annealing treatment with a multistep process: 250 °C for 10 min (with a heating rate of 10 °C/min), 300 °C for 5 min, 450 °C for 2 min, and then cooling down at a rate of 10 °C/min. For the fabrication of perovskite solar cells, a non-stoichiometric precursor solution containing CH_3NH_3I and lead(II) Chloride ($PbCl_2$, 1.0 mol/L) in a molar ratio of 3:1.03 in DMF was spin-coated on the thin TiO_2 electrodes at 3000 rpm for 30 s [53]. After spin-coating, the films were dried at room temperature in the glove box for 30 minutes to evaporate solvent and to form a highly continuous films prior to annealing at 105 °C for 90 min [54]. After cooling down, a hole-transporting material (HTM) solution comprised of 61 mM spiro-OMeTAD, 55 mM tert-butylpyridine (TBP) and 26 mM Li-TFSI salt in chlorobenzene was spin-coated on the perovskite layer at 4000 rpm for 30 s. The electrodes were then put into a desiccator overnight. Finally, the top electrodes were deposited by thermal evaporation of a 100-nm-thick Au layer onto the masked electrodes. The active area for the PSCs is 0.08 cm^{-2}.

2.5 Electromagnetic simulations

The full-wave simulations were conducted with a commercial finite-element solver (Comsol Multiphysics 4.3a with RF module), which is commonly used to simulate the LSPR of plasmonic nanoparticles. When performing the numerical simulations, the total-field scattering-field source was used to get the extinction cross sections as well as the electric field distributions at the longitudinal and transverse resonant wavelengths. In all calculations, the frequency dependent permittivity of Au and Ag were modeled using the experimental data of Johnson and Christy with linear interpolation. The simulation domain was finely meshed with the smallest size of 1.5 nm in the metal region to ensure the accuracy of the calculated results.

2.6 Measurements and Characterization

The optical properties of the perovskite electrodes, extinction behavior of the plasmonic AuNRs and Au@Ag were investigated by a UV-Vis spectrophotometer (Hitachi U-3010, Japan) equipped with an integrating sphere. The structural morphologies of the AuNRs and Au@Ag were studied by transmission electron microscope (TEM, JEOL JEM-2100F). I–V curves were recorded using a Keithley 2420 source meter. The 1 Sun AM 1.5 G illumination (100 mW cm^{-2}) was supplied by a 300 W solar simulator (Model 69911, Newport-Oriel Instruments, USA) and calibrated by a silicon reference cell (NIST) equipped with a power meter. The IPCE measurements were conducted on a Newport 2931-C power meter, employing a light source provided by a Newport 66902 solar simulator equipment with a Newport 74125 monochromator.

3. Results and discussion

3.1 Structural and optical properties of Au@Ag core-shell nanocuboids

Au@Ag core-shell nanocuboids were prepared through a chemical bath routine. First, uniform Au nanorods (AuNRs) with 55 ± 2.5 nm in length and 11.5 ± 0.5 nm in width (Fig. S1, Supporting Information) were synthesized using the hexadecyl trimethyl ammonium bromide (CTAB) cationic surfactant as morphology controller. In the second step, Ag shells were grown on the surface of the AuNRs, forming the Au@Ag core-shell nanocuboid architecture with rectangular edges and vertices. The thickness of the Ag shell was readily controlled by tuning the added amount of AgNO$_3$ (*i.e.* 400, 800, 1200 and 1600 μL, 0.01 M). **Fig. 1**a-d shows the transmission electron microscopy (TEM) images of the as-prepared Au@Ag nanocuboids with varied Ag shell thickness. The detailed structural parameters are summarized in Table S2 (Supporting Information). Briefly, the reduction of Ag$^+$ at the two ends of a nanorod is more slowly than at the lateral sides, leading to an anisotropic growth of the Au@Ag nanocuboid, which is consistent with reported work [45]. The Ag thickness along the minor axis increases remarkably from 10 ± 0.7 to 25 ± 1.0 nm, whereas that along the

9
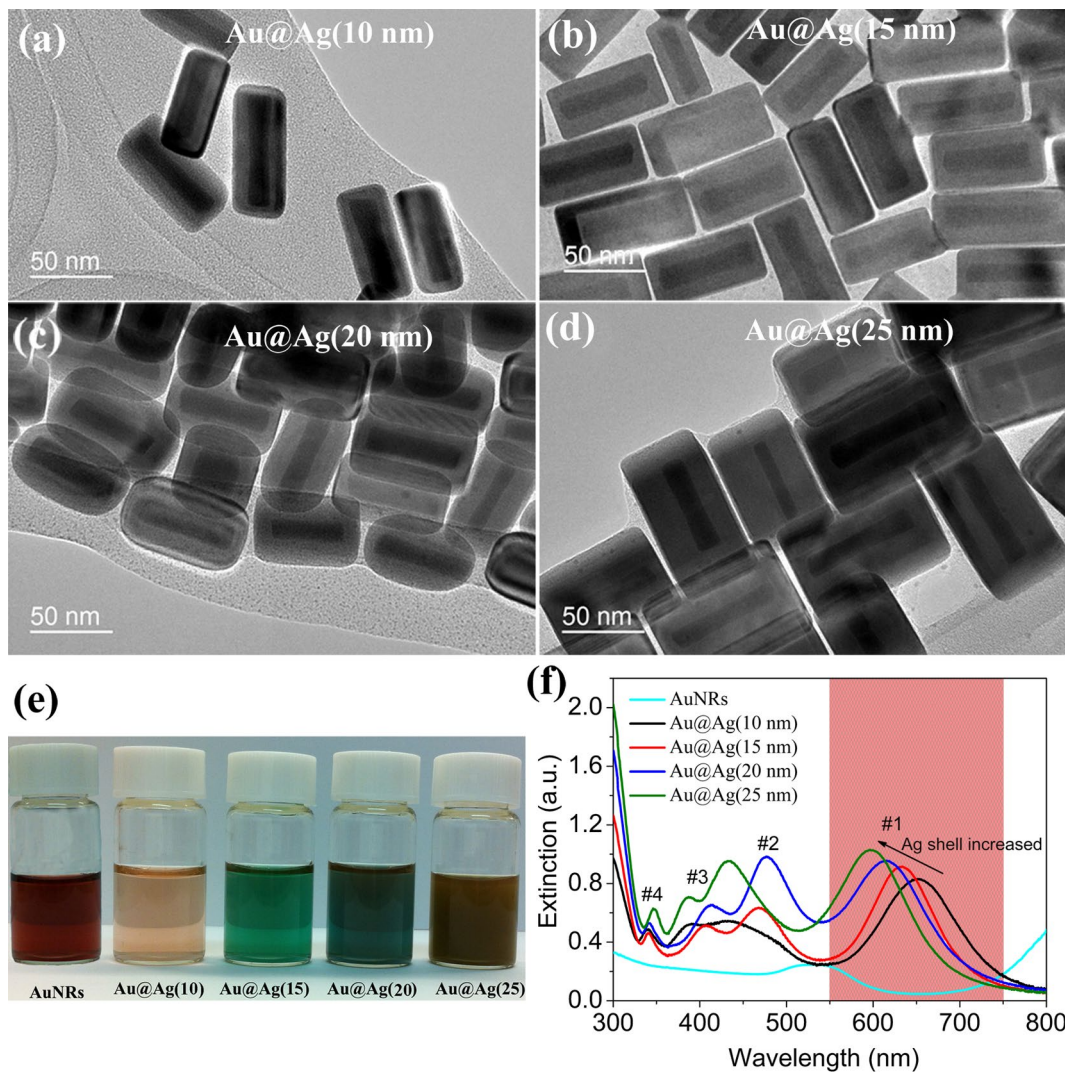
Fig. 1 (a-d) TEM images of the Au@Ag core-shell nanocuboids: Au@Ag (10 nm), Au@Ag (15 nm), Au@Ag (20 nm), Au@Ag (25 nm), respectively, with the Ag shell thickness in parenthesis. The Au nanorods core has a dimension of 55 nm × 11 nm (length × width). (e) Optical photographs showing the color changes of the Au@Ag core-shell nanocuboid colloids with increasing Ag shell thickness. (f) Extinction spectra of the AuNRs and Au@Ag nanocuboids with varied Ag shell thickness in aqueous solution with the same Au concentration of ~2×10^{-10} M.

major axis elongates from 6.0 ± 0.5 to 10.5 ± 1.0 nm, when the added amount of AgNO$_3$ increases from 400 to 1600 µL. Due to the asymmetric growth of the Ag nanoshell, the length of the Au@Ag capsule increases from 68.5 to 89.1 nm, while the width increases dramatically from 30.5 to 60.4 nm, leading to the aspect ratio declining from 2.2 to 1.4. The structure evolution of the Au@Ag nanocuboids is accompanied by remarkable changes in their

plasmonic properties. As the Ag thickness increases, the nanocuboid solution changes its color from red to blue and finally to purple (Fig. 1e). The extinction spectra reveal that the AuNRs show two absorption peaks located at 531 and 852 nm (Fig. 1f and Fig. S2), corresponding to the transverse and longitudinal LSPR modes, respectively [44-46]. Upon Ag coating, the lowest-energy plasmon band is gradually blue-shifted and new plasmon bands are generated simultaneously at higher energies [44,48]. Typically, four LSPR peaks (numbered as peaks #1-4 from low to high energies sequentially) appear in the Au@Ag extinction spectra (Fig. 1f). Taking Au@Ag(15 nm) for instance, the peak #1 at ~631 nm can be ascribed to the longitudinal dipolar plasmon mode and the peak #2 (~468 nm) to the transverse dipolar plasmon mode of the Au@Ag nanocuboids [44,48]. The two higher-energy peaks at 410 and 341 nm can be ascribed to the octupolar plasmon modes of the Ag shell [44,45,48]. The peak positions of the four plasmon bands, especially the two lower-energy ones, are strongly dependent on the aspect ratio of the nanocuboid. Specifically, the extinction peak #1 blue-shifts continuously from 651 to 595 nm (i.e., 651, 631, 616 and 595 nm) when the aspect ratio decreases from 2.2 to 1.4 (the corresponding Ag shell thickness along the minor axis increases from 10 to 25 nm). A comparison of the extinction spectra demonstrates clearly that the LSPR extinction intensities of all Au@Ag nanocuboids are significantly higher than that of the AuNRs in the wavelength range of 300-720 nm. Taking the Au@Ag(15 nm) nanocuboids for instance, the extinction intensities at 480 and 616 nm are 5 and 12 times that of the AuNRs, respectively. Even the lowest extinction intensity of the Au@Ag nanocuboids at 540 nm is comparable to that of the bare AuNRs. More importantly, the LSPR extinction bands of the Au@Ag nanocuboids extends to around 750 nm, which are much broader than that of conventional Au or Ag nanospheres.

3.2 Broadband plasmonic absorption enhancement in Au@Ag incorporated PSCs
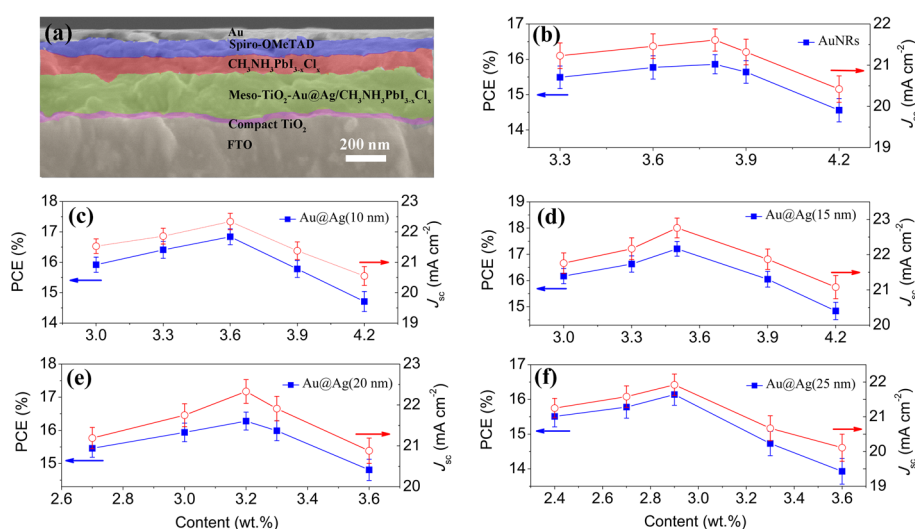
Fig. 2 (a) Cross-section SEM image of the Au@Ag nanocuboids incorporated perovskite solar cell. (b-f) PCE and short-circuit current density (J_{sc}) of the PSCs as a function of the incorporated plasmonic nanoparticle concentration. The error bars represent the standard deviation of nine devices prepared under each condition.

For preventing structural damage from thermal treatment, a thin TiO_2 layer with a thickness around 3 nm was coated on the AuNRs and Au@Ag samples by dipping the AuNRs or Au@Ag incorporated thin TiO_2 films into a titanium isopropoxide (TTIP) based solution, followed by a sophisticated fast-annealing process. The measured extinction spectra (Fig. S3, Supporting Information) demonstrate that the fast-annealing process did not degrade the optical property of the Au@Ag nanocuboids with the protective thin TiO_2 shells. The scanning electron microscope (SEM) images (Fig. S4, Supporting Information) reveals that the Au@Ag nanocuboids are distributed uniformly in the mesoporous TiO_2 film without any aggregation. The concentration of Au@Ag incorporated in the mesoscopic $TiO_2/CH_3NH_3PbI_{3-x}Cl_x$ layer of the prepared PSCs (**Fig. 2**a) was optimized individually to achieve maximized enhancement in device efficiency. The optimized contents of AuNRs, Au@Ag(10 nm), Au@Ag(15 nm), Au@Ag(20 nm), and Au@Ag(25 nm) in the photoactive layer are 3.8, 3.6, 3.5, 3.2, and 2.9 wt%, respectively (Fig. 2d-f, Table S3.1-3.5, Supporting Information).

Fig. 3a shows the *J-V* curves (reverse scanning, from photovoltage to short-circuit current) of the optimized devices and the corresponding photovoltaic parameters are tabulated in **Table 1** for direct comparison. Control device was fabricated on the bare TiO_2 electrode without inclusion of any metal NPs, which demonstrates a short-circuit current density (J_{sc}) of 20.68 mA/cm^2, an open-circuit photovoltage (V_{oc}) of 1.0 V and a fill factor (*FF*) of 0.731, leading to a PCE of 15.16%. By adding 3.8 wt.% of Au NRs into the photoactive layer, a PCE of 15.86% (4.6% enhancement) was achieved, with corresponding J_{sc}, V_{oc} and *FF* of 21.61 mA/cm^2, 1.00 V and 0.735, respectively. Surprisingly, when the Au@Ag nanocuboids with intense and broad LSPR bands are incorporated into the devices, the J_{sc} boosts significantly to 21.92~22.76 mA/cm^2, yielding PCE of 16.89%, 17.21%, 16.35%, and 16.14% for the Au@Ag(10 nm), Au@Ag(15 nm), Au@Ag(20 nm), and Au@Ag(25 nm) based devices, respectively, corresponding to efficiency enhancement of 11.4%, 13.5%, 7.8%, and 6.5%, respectively. These values are significantly larger than the enhancement caused by the AuNRs, which are mainly attributed to the remarkable increase in J_{sc}, as shown in Table 1.

To reveal the factors governing the J_{sc} and PCE enhancement, further studies were carried out by measuring the optical properties of the thin perovskite films deposited on various plasmonic NP incorporated TiO_2 films. As shown in Fig. 3b, the $CH_3NH_3PbI_{3-x}Cl_x$ sensitizer exhibits strong light extinction in the λ_{Hi} range of 400-600 nm, whereas the light absorption becomes relative weak in the λ_{Lo} zone. The absorption spectra of the $CH_3NH_3PbI_{3-x}Cl_x$ electrodes with the addition of plasmonic nanocuboids witness only a slight absorption improvement in the λ_{Hi} region for all the cases, in spite of the fact that both Au nanorods and Au@Ag nanocuboids demonstrate a considerable LSPR response in this zone. This result is consistent with that reported by Snaith [41,42] and the strong light extinction capacity of $CH_3NH_3PbI_{3-x}Cl_x$ over this wavelength zone is responsible for the inconspicuous enhancement of light absorption [43]. However, considerable improvement in light absorption is observed in the long wavelength zone (550-750 nm) for the Au@Ag incorporated films.
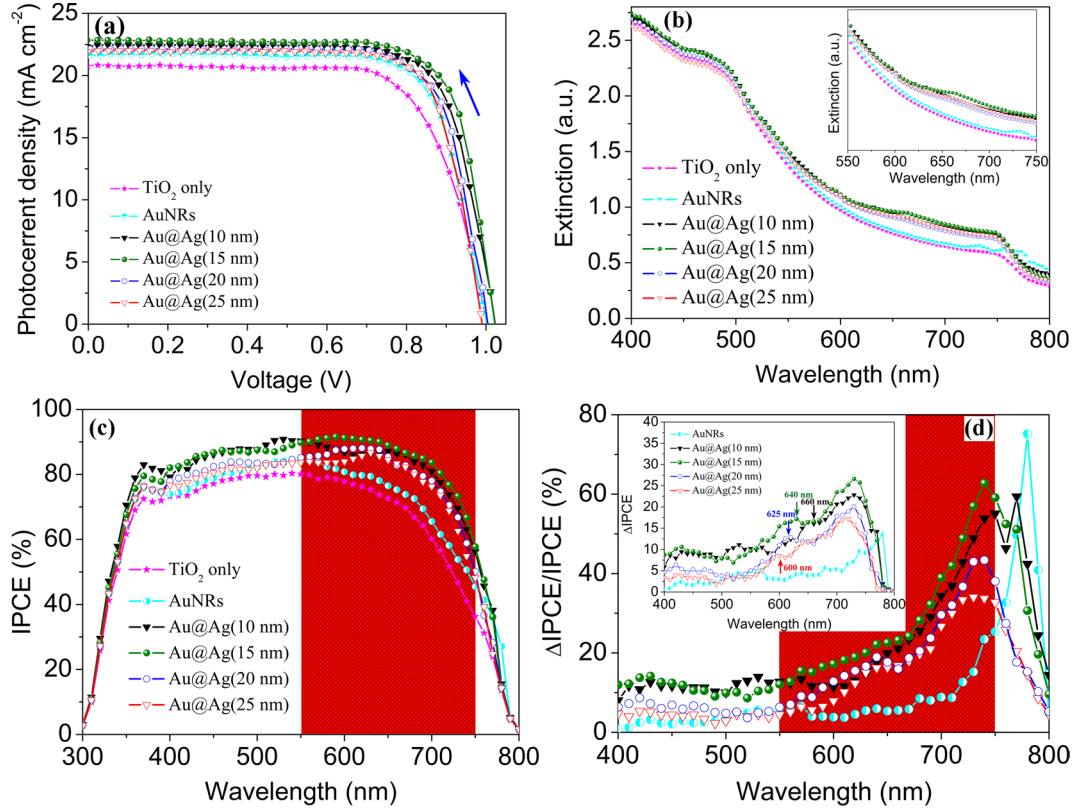
Fig. 3 (a) *J-V* curves of perovskite devices based on TiO_2 mesoscopic, AuNRs and different Au@Ag incorporated electrodes. (b) UV-Vis absorption spectra of the $CH_3NH_3PbI_{3-x}Cl_x$ perovskite electrodes deposited on pure TiO_2 film and TiO_2 films with AuNRs or Au@Ag incorporation. (c) IPCE spectra and (d) relative IPCE enhancement ratio (ΔIPCE/IPCE) and ΔIPCE (inset) of the perovskite solar cells based on pure TiO_2 film and TiO_2 films with AuNRs or various Au@Ag nanocuboids.

Table 1. Photovoltaic parameters of the perovskite solar cells with various photoanodes [a)]

Devices	J_{sc} [mA/cm^2]	V_{oc} [V]	FF	PCE [%]	ΔPCE/PCE	$J_{sc\,(550-750\,nm)}$[b)] [mA cm^{-2}]
TiO_2 only	20.68±0.45	1.0±0.01	0.731±0.01	15.16±0.4		11.34
AuNRs	21.61±0.50	1.0±0.02	0.735±0.015	15.86±0.5	4.6%	11.68
Au@Ag(10 nm)	22.46±0.46	1.02±0.02	0.739±0.015	16.89±0.5	11.4%	12.59
Au@Ag(15 nm)	22.76±0.50	1.02±0.02	0.741±0.01	17.21±0.45	13.5%	12.93
Au@Ag(20 nm)	22.13±0.63	1.0±0.03	0.739±0.02	16.35±0.65	7.8%	12.32
Au@Ag(25 nm)	21.92±0.72	0.994±0.04	0.736±0.03	16.14±0.75	6.5%	12.27

This relatively strong enhancement in absorbance results from the relatively poor light extinction of $CH_3NH_3PbI_{3-x}Cl_x$ and strong LSPR absorbance of the Au@Ag nanocuboids in this wavelength region (Fig. S5 and S6, Supporting Information). These features suggest that the Au@Ag nanocuboids with broadband and strong LSPR have facilitated the $CH_3NH_3PbI_{3-x}Cl_x$ sensitizer located in the vicinity of Au@Ag to absorb more low-energy photons due to the intensified near-field effect of the plasmonic nanostructures. This remarkably enhanced light harvesting capacity in the λ_{Lo} range ultimately leads to an effective increase in the photocurrent and the efficiency of the solar cells, as shown in Fig. 3a and Table 1. The curves in Fig. 3b and Fig. S6 (Supporting Information) witness the best light absorption enhancement of the perovskite electrode with Au@Ag(15 nm) plasmonic metal nanoparticle incorporation, which is one of the key factors for the best J_{sc} boosting and the highest PCE. The remarkable improvement in light harvesting of Au@Ag(15 nm) incorporated electrodes is resulted from both the considerable LSPR extinction at the 550-750 nm zone and the strong intensified near-filed effects which will be discussed later.

As compared with UV-Vis light absorption, the IPCE is more pertinent to the photocurrent generation in solar cells, since it takes the incident light harvesting efficiency, electron injection, and charge collection efficiency into a comprehensive consideration. The IPCE spectra and the relative IPCE enhancement ratio (ΔIPCE/IPCE) as a function of wavelength are displayed in Fig. 3c and Fig. 3d, respectively. The relative IPCE enhancement (ΔIPCE) is also illustrated as an inset of Fig. 3d to show more details about the IPCE variation induced by the incorporation of different Au@Ag nanocuboids. It reveals that the devices without any plasmonic metal particle incorporation exhibit a relative low IPCE and a remarkable IPCE decline at the wavelength range of 600-800 nm, due to the relative low light extinction capacity at this zone and thin perovskite film used (around 280 nm, Fig. 2a). All devices

incorporated with plasmonic NRs demonstrate a considerable IPCE enhancement over 400-750 nm. A much remarkable increase in IPCE is observed in the λ_{Lo} range (shaded zone as shown in Fig. 3c and 3d) for the Au@Ag incorporated cells, as compared with the enhancement at λ_{Hi}. For instance, the IPCE of the Au@Ag(15 nm) cell is increased by ~40% and 60% at 700 nm and 750 nm, respectively, in contrast to only 10.2% at 500 nm. The ΔIPCE shown as inset of Fig. 3d illustrates a wavelength-dependent IPCE increase, the ΔIPCE at the zone where the Au@Ag (X nm, X=10, 15, 20 or 25) shows the highest light extinction is obviously larger than that of its near-neighbor, indicating a real plasmonic effect based improvement. However, this wavelength-dependent IPCE variation is not as significant as wavelength-dependent light extinction of Au@Ag shown in Fig. 1f. Several reasons may be response for this result: (i) the extinction curve (Fig. 1f) of the Au@Ag nanocuboids includes both the absorption and scattering contributions (Fig. S5-7), where the latter takes up a larger portion and gives less positive contribution to the light harvesting in this device configuration (will show later); (ii) IPCE is related to not only the light harvesting efficiency but also the electron injection and charge collection efficiency, with the latter two being affected by the near field effect of plasmonic particles [41,42]; (iii) The spectra dependence of ΔIPCE/IPCE is even more complicated, with a smaller IPCE of the control device normally leading to a higher ΔIPCE/IPCE value. As shown in Table 1, the J_{sc} integrated from the IPCE spectra within the long wavelength range (550-750 nm) is 11.34 mA cm^{-2} for the pristine cells, which increases to 12.93 mA cm^{-2} for the Au@Ag(15 nm) based devices. The increase of integrated J_{sc} (1.59 mA cm^{-2}) from the low energy zone (550-750 nm) takes up the major share of the total J_{sc} improvement (2.2 mA cm^{-2}, measured from J-V curves). Therefore, it can be concluded that the remarkable enhancement of IPCE in the λ_{Lo} range makes the most significant contribution to the boosted J_{sc} and PCE of the Au@Ag incorporated solar cells.

To fully elaborate the LSPR effects of Au@Ag on PSCs, **Fig. 4** plots the distributions of the electric field intensity on the transvers cross-sections of different structures at their

16
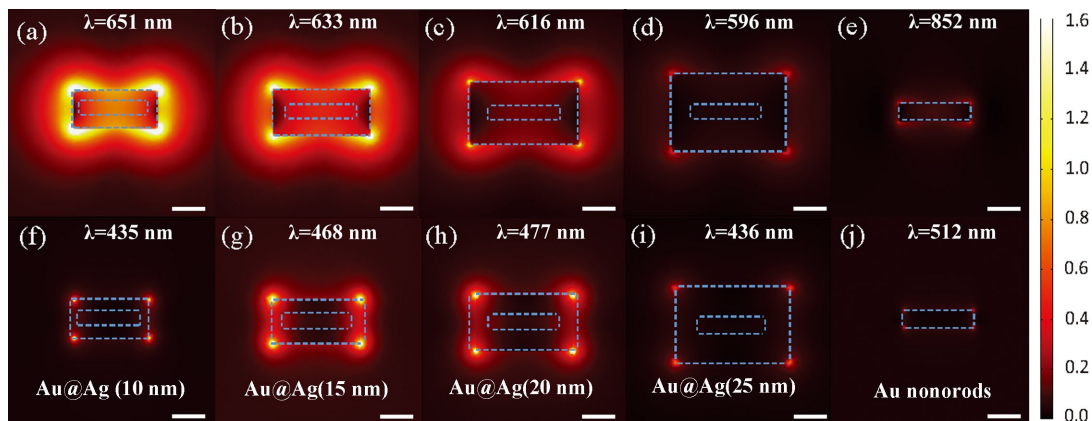
Fig. 4 Simulated electric field distribution at corresponding resonance wavelengths for Au@Ag with varied Ag shell thickness: (a-e) longitudinal dipolar mode and (f-j) transverse dipolar mode, with the resonance wavelengths indicated in the Fig.s. The structures from left to right are Au@Ag(10 nm), Au@Ag(15 nm), Au@Ag(20 nm), Au@Ag(25 nm) and AuNR, respectively. The scale bars in all panels are 25 nm. The intensity enhancement contours are drawn in a logarithmic scale. The dashed lines show the boundaries between two different materials.

longitudinal and transverse resonant wavelengths, respectively. It is found that, the near field intensity for the longitudinal mode is increased by around 20 times upon the coating of an Ag shell (*i.e.* 10 nm and 15 nm) on an Au nanorod (Fig. 4a, 4b and 4e). Meanwhile, the simulated field patterns shown in Fig. 4 also reveal that the plasmonic electric field can extend to tens of nanometers from the surface of the Au@Ag (especially for Au@Ag(10 nm) and Au@Ag(15 nm)) to the perovskite, while the electric field is localized within a few nanometers around the AuNR. Considering the near-field nature of the plasmonic enhancement, a broader space distribution of the enhanced electric field will result in more light-harvesting. The significant enhancement in the near field intensity is another key factor that enhances the light harvesting and IPCE of the Au@Ag incorporated PSCs, apart from their stronger and tunable LSPR bands in comparison with the AuNRs. The simulated extinction spectra of the different Au@Ag (Fig. S5, Supporting Information) demonstrate a continuous increase in extinction intensity (a far-field effect) with increasing Ag shell thickness, consistent with the measured spectra of the Au@Ag NPs in water (Fig. 1f). However, as shown in Fig. 4, both the near-

field intensity and the field distribution size of longitudinal dipolar mode begin to decline significantly when the Ag shell thickness is larger than 15 nm (Fig. 4a-d), while the near field intensity and the field distribution size of the transverse dipolar mode first increase with increasing Ag shell thickness and then starts to decrease remarkably. Two reasons are responsible for this effect: (1) the electric field is stronger where the radius of curvature of a nanoparticle is smaller, as the electric field is proportional to the density of electrons; (2) moreover, by comparing with monometallic Au/Ag nanoparticles, core-shell type bimetallic Au@Ag nanoparticles have more LSPR modes and larger electric near field because of the synergistic effect of metal components and plasmon coupling from different metallic interfaces [42-45]. As shown in Fig. 4f-j, the Au@Ag (15 nm) exhibits the strongest near field intensity and the largest field distribution size of transverse dipolar mode, while its near field intensity and field distribution size of the longitudinal dipolar mode is only slightly less than that of Au@Ag (10 nm). Additionally, the extinction of Au@Ag (15 nm) is also slightly stronger than Au@Ag (10 nm) (Fig. 1f). Therefore, a higher efficiency is observed for the Au@Ag (15 nm) incorporated device.

3.3 Device optimization: effective light scattering management

To maximize the cell efficiency and fully explore the efficient light management effect of the Au@Ag nanocuboids in the PSCs, four devices in different configurations were constructed and characterized (**Fig. 5**a-d). In the design of device architecture, the Au@Ag(15 nm) was firstly chosen to be imbedded in the mesopourous layer (3.5 wt.% incorporation) since it gives the best photovoltaic performance in this type of architecture as demonstrated above, while the Au@Ag(20 nm) was chosen to be the scattering material since it possesses simultaneously large light scattering (Fig. S7, Supporting Information), high light extinction (Fig. 1f and Fig. S5) and good near-field effect (Fig. 4). The *J-V*, IPCE and ΔIPCE/IPCE results of the four devices are displayed in Fig. 5e-f and the detailed photovoltaic parameters are summarized in **Table 2**. It can be seen that the deposition of Au@Ag(15 nm) nanocuboids
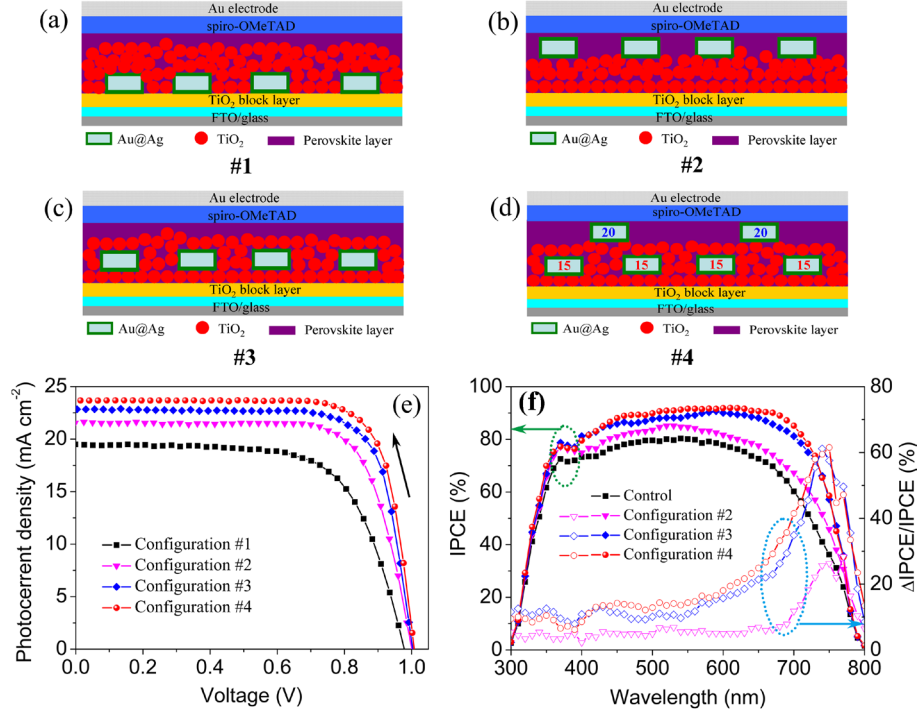
Fig. 5 (a-d) Schematic diagrams of the Au@Ag core-shell nanocuboid incorporated PSCs with the Au@Ag layer below (#1), on the top of (#2), embedded in (#3), and both embedded in and on the top of (#4) the TiO₂ mesoscopic layer, respectively. (e) *J-V* characteristic curves of PSCs with four kinds of configurations. (f) Wavelength dependent IPCE (solid symbols) and relative IPCE enhancement ratio (ΔIPCE/IPCE, open symbols) of the cells in different configurations.

Table 2. Photovoltaic parameters of the perovskite solar cells incorporated with the Au@Ag nanocuboids in different configurations[a]

Devices	J_{sc} [mA/cm²]	V_{oc} [V]	FF	PCE [%]	ΔPCE/PCE	IPCE$_{550-750}$/IPCE
Bare TiO₂	20.68±0.45	1.0±0.01	0.731±0.01	15.16±0.40		41.9%
ConFig. #1	19.45±1.10	0.955±0.05	0.675±0.03	12.53±1.20	-17.1%	40.9%
ConFig. #2	21.78±0.55	1.01±0.02	0.735±0.02	16.16±0.50	6.7%	43.7%
ConFig. #3	22.76±0.50	1.02±0.02	0.741±0.01	17.21±0.45	13.5%	46.9%
ConFig. #4	23.35±0.50	1.04±0.02	0.737±0.02	17.83±0.45	17.6%	47.9%

[a] Average values obtained from at least 5 independent cells. The data for bare TiO₂ and Au@Ag (15 nm) based cells (namely configuration #3) shown in Table 1 were relisted here for a convenient comparison.

below the TiO_2 mesoscopic layer deteriorates the device performance when compared with the bare TiO_2 cells. This is due to the dual effects of the Au@Ag nanocuboids in front of the photoactive layer that scatter the incident photons out of the device and also impede the effective connection between the perovskite and the electron transport layer (compact TiO_2 layer), leading to direct light loss and less efficient charge transfer from the perovskite layer to the current collecting electrode. When the Au@Ag(20 nm) nanocuboids were deposited on the top of the mesoporous TiO_2 layer (configuration #2, Fig. S8, Supporting Information) and act as scattering material, the device demonstrates J_{sc}, V_{oc}, FF and PCE of 21.78 mA/cm^2, 1.01 V, 0.735 and 16.17%, respectively, corresponding to an enhancement of 6.7% in PCE. For the configuration #3, namely the optimized structure in Fig. 2d, the J_{sc}, V_{oc} and FF are 22.76 mA/cm^2, 1.02 V and 0.741, respectively, and an impressive PCE of 17.21% is yielded, leading to a PCE enhancement of 13.5% which is much greater than the devices in the configurations #1 and #2.

In addition to the LSPR enhanced low-energy absorption, the Au@Ag nanocuboids also exhibit considerable light scattering effect (Fig. S7, Supporting Information). To investigate the plasmon-enhanced light scattering effect of the Au@Ag nanocuboids on the cell performance independently, we performed a control experiment by incorporating 3.5 wt.% non-plasmonic TiO_2 nanocuboids with similar size (~80 nm in length) into the electrode to replace the Au@Ag(20 nm) in configuration #2 or Au@Ag(15 nm) in configuration #3. For the TiO_2 nanocuboids incorporated cell in configuration #3, the photovoltaic performance (Fig. S9 and Table S4, Supporting Information) shows that the PCE is slightly declined by 4.1%. For configuration #2, the J_{sc} was increased from 20.56 to 21.21 mA/cm^2 and an efficiency enhancement of 3.6% was obtained, due to the back scattering of photons to the mesoporous TiO_2/perovskite layer in this architecture. These results point out that the slight light scattering effect induced by the nanocuboids (tens of nanometers in size) in the very thin mesoporous TiO_2/perovskite film (configuration #3) is offset by the slightly reduced

perovskite loading (nanocuboids have much smaller specific surface area than the mesoporous TiO$_2$ nanoparticles) and gives rise to no positive contribution to the enhancement of J_{sc} and PCE. By comparing the photovoltaic performance of Au@Ag (6.7% enhancement) and TiO$_2$ nanorod (3.6% enhancement) incorporated devices with the same configuration #2, we can deduce that both LSPR enhanced low-energy absorption and light scattering effect are responsible for the improved performance of the device with this type of architecture. Since the LSPR enhanced absorption demonstrates the best performance in configuration #3 and the scattering effect works more efficiently in configuration #2, we further optimized the device structure with configuration #4 and the concentrations of Au@Ag(15 nm) in TiO$_2$ mesoporous layer and Au@Ag(20 nm) on the top of TiO$_2$ scaffold was synthetically optimized at 3.2 wt% and 1μm^{-2} (Table S5.1 and S5.2, Fig.S8). A more significant enhancement in J_{sc} was observed, leading to a higher PCE of 17.83%, with a J_{sc} of 23.35 mA/cm^2, V_{oc} of 1.04 V and FF of 0.737. The relative PCE enhancement ratio is 17.6%, compared with the device without plasmonic particles.

The IPCE spectra and relative IPCE enhancement ratio of the Au@Ag incorporated PSCs with different configurations are displayed in Fig. 5f. Obviously, all devices with configurations #2, #3 and #4 show a remarkable IPCE increase in the zone of 550-750 nm, owing to their strong LSPR extinction band in this range. The differences of IPCE and ΔIPCE/IPCE between configurations #3 and #4 in the zone of 480-550 nm where the LSPR extinction are relatively weak (Fig. 1f) are presumably duo to the light scattering effect of the Au@Ag(20 nm) capsules on top of the TiO$_2$ mesoscopic layer. For the configurations #3 and #4, a significant ΔIPCE/IPCE improvement (20-60%, wavelength dependent) in the λ_{Lo} range of 550-750 nm is obtained, while it is around 15% in the λ_{Hi} zone of 300-550 nm (Fig. 5f). To further quantify the improvement, we integrated and compared the IPCE in the range of 550-750 nm and the whole spectrum. The IPCE$_{550-750}$/IPCE represents the ratio of contribution from the 550-750 nm region to the whole IPCE, indicating the capacity of the hybrid PSCs to

utilize the λ_{Lo} sunlight. As listed in Table 2, the $IPCE_{550-750}/IPCE$ of the control devices without Au@Ag is 41.9%, showing that the IPCE contribution from λ_{Lo} illumination is not the major part. With the incorporation of Au@Ag (15 nm), the $IPCE_{550-750}/IPCE$ is remarkably increased to 46.9% and 47.8% for the devices with configurations #3 and #4, respectively. Those results coherently demonstrate that the inclusion of the plasmonic Au@Ag core-shell nanocuboids with strong, broadband and tunable LSPR extinction into the active layer is a promising approach to increase the utilization of low-energy photons, leading to efficient panchromatic PSCs with improved light harvesting efficiency. Meanwhile, exploiting the light scattering effect *via* a reasonable structure can further enhance the photovoltaic performance, leading to a dual-enhancement effect of the plasmonic metal nanoparticles incorporated PSCs.

To evaluate the reproducibility of the Au@Ag (15 nm) incorporated PSCs constructed with the configuration #4, 30 devices were tested. The histograms of the PCE performance is presented in **Fig. 6**a. It can be seen that the PCE is centered at around 17.5% (17.83% of the average PCE), with 5 cells showing PCE lower than 16.5% and 2 devices over 18%. The standard deviations of PCE over 30 devices is 0.516. The champion device demonstrates a high PCE up to 18.31%, with J_{sc}, V_{oc} and *FF* of 23.60 mA cm^{-2}, 1.04 V and 0.746, respectively (Fig. 6b). In general, using the Au@Ag nanocuboids with broadened absorption band, stronger extinction capacity, significantly improved near-field effects and effective light scattering management one can obtain efficient plasma enhanced PSCs with relatively high average PCE.
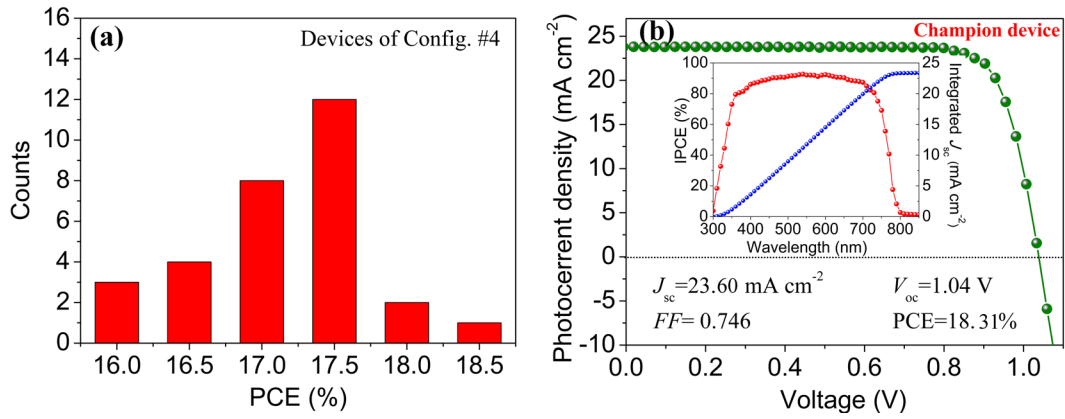
Fig. 6 (a) Statistics of 30 devices showing an average PCE ~17.5% and a standard deviation (S.D.) of 0.516. (b) Performance of the champion PSC constructed in configuration #4. Inset: IPCE and the integrated photocurrent over wavelength.

3.4 Photoluminescence, stability and hysteresis behaviors of the devices

To fully reveal the mechanism, apart from the plasmonic enhanced light-harvesting, of Au@Ag nanocuboids for improving the performance of PSCs, the steady-state photoluminescence (PL) and time-resolved PL (tr-PL) spectra of Au@Ag nanocuboids incoporated perovskite electrode (configuration #4) and its reference film were recorded to understand the role of Au@Ag nanocuboids on the carrier dynamics. As shown in Fig.S10a, with the presence of Au@Ag, a remarkable reduction of PL intensity is observed, and the PL decay lifetime is decreased from 28.6 ns to 12.5 ns (Fig.S10b). The fast PL quenching and declined decay lifetime indicates the more efficient electron-hole seperation, enhanced carriers extraction at the perovskite/TiO$_2$ interface. The efficient electron-hole seperation will accelerate the perovskite regeneration, while fast carrier extraction can suppress the charge recombination, both of which will also lead to the improvement of the PCE of the devices. These results are similar the work reported by Snaith and Bardhan [41,42,55].

Beside the efficiency, the stability and hysteresis are also important issues to be concerned for PSCs. The device with TiO$_2$ coated Au@Ag shows a similar stability behavior to the one without any metal plasmonic particles (Fig. S11, Supporting Information), indicating that the incorporation of TiO$_2$ coated Au@Ag will neither deteriorate nor improve

23

the stability of the devices. The TiO$_2$ layer plays an important role of resisting the corrosion of Ag by the perovskite. The hysteresis is always an open issue of PSCs. We have also investigated the influence of Au@Ag nanocuboids on the hysteresis of the devices. Interestingly, the addition of the Au@Ag nanocuboids can reduce the hysteresis to a certain degree (Fig. S12, Supporting Information). According to Park's method, the J-V hysteresis can be quantified using the hysteresis index (HI) described by the following equation:[56]

$$HI = \frac{J_{RS}(0.8V_{oc}) - J_{FS}(0.8V_{oc})}{J_{RS}(0.8V_{oc})}$$

where $J_{RS}(0.8V_{oc})$ and $J_{FS}(0.8V_{oc})$ are the photocurrent densities at 80% of the V_{oc} for reverse and forward J-V scans, respectively. The HI is caculated to be 0.168 and 0.544 for the Au@Ag (15 nm) incorporated and pristine devices, respectively. The alleviated hysteresis for plasmonic based device may arise from two reasons: (1) the Au@Ag can accelerated exciton dissociation [42]; (2) the metal particles can reduce the film resistance and improve the electron transport [38], resulting in decreased charge accumulation at the TiO$_2$/perovskite interface.

4. Conclusion

In summary, Au@Ag core-shell nanocuboids with intense, tunable and broadband localized surface plasmon resonances were successfully synthesized and incorporated in CH$_3$NH$_3$PbI$_{3-x}$Cl$_x$ perovskite solar cells. By matching the plasmon resonance band of Au@Ag with the low-energy absorption edge of the sensitizer, the light harvesting efficiency of the plasmonic perovskite solar cells shows remarkable improvement as manifested by significant increase in the device's short-circuit current. A rational utilization of the light scattering effect of the Au@Ag nanocuboids can further enhance the light harvesting efficiency and hence the device performance. As a result, an overall PCE of 18.31% was achieved for a champion hybrid perovskite solar cell, corresponding to an efficiency enhancement of 20.8%. An average PCE of 17.83% over 30 individual devices witnesses the success of using the Au@Ag core-shell

plasma to remarkably improve the performance of PSCs. Our approach towards panchromatic sunlight harvesting is also applicable to other types of solar cells and light-driven devices, such as, artificial photosynthesis and solar thermal energy harvesting, due to the fact that the localized surface plasmon bands can be easily manipulated to match the absorption band of most photoactive materials.

Appendix A. Supplementary material

Supplementary data associated with this article can be found in the online version at

References

[1] J. Burschka, N. Pellet, S.J. Moon, R. Humphry-Baker, P. Gao, M.K. Nazeeruddin, M. Grätzel, Nature 499 (2013) 316.

[2] M.Z. Liu, M.B. Johnston, H.J. Snaith, Nature 501 (2013) 395.

[3] H.J. Snaith, J. Phys. Chem. Lett. 4 (2013) 3623.

[4] H.P. Zhou, Q. Chen, G. Li, S. Luo, T.B. Song, H.S. Duan, Z.R. Hong, J.B. You, Y.S. Liu, Y. Yang, Science 345 (2014) 542.

[5] C.S. Ponseca, T.J. Savenije, M. Abdellah, K.B. Zheng, A. Yartsev, T. Pascher, T. Harlang, P. Chabera, T. Pullerits, A. Stepanov, J.P. Wolf, V. Sundström, J. Am. Chem. Soc. 136 (2014) 5189.

[6] P.P. Boix, K. Nonomura, N. Mathews, S.G. Mhaisalkar, Mater. Today 17 (2014) 16.

[7] S.D. Stranks, P.K. Nayak, W. Zhang, T. Stergiopoulos, H.J. Snaith, Angew. Chem. Int. Ed. 54 (2015) 3240.

[8] Z.H. Wei, H.N. Chen, K.Y. Yan, S.H. Yang, Angew. Chem. Int. Ed. 53 (2014) 13239.

[9] T.M. Schmidt, T.T. Larsen-Olsen, J.E. Carlé, D. Angmo, F.C. Krebs, Adv. Energy Mater. 5 (2015) 1500569.

[10] M. Saliba, T. Matsui, J.Y. Seo, K. Domanski, J.P. Correa-Baena, M.K. Nazeeruddin, S.M. Zakeeruddin, W. Tress, A. Abate, A. Hagfeldtd, M. Grätzel, Energy Environ. Sci. 9 (2016) 1989.

[11] X. Li, D.Q. Bi, C.Y. Yi, J.D. Décoppet, J.S. Luo, S.M. Zakeeruddin, A. Hagfeldt, M. Grätzel, Science 353 (2016) 58.

[12] W.S. Yang, J.H. Noh, N.J. Jeon, Y.C. Kim, S. Ryu, J. Seo, S. Il Seok, Science 348 (2015) 1234.

[13] Y. Ogomi, A. Morita, S. Tsukamoto, T. Saitho, N. Fujikawa, Q. Shen, T. Toyoda, K. Yoshino, S.S. Pandey, T.L. Ma, S. Hayase, J. Phys. Chem. Lett. 5 (2014) 1004.

[14] G.E. Eperon, S.D. Stranks, C. Menelaou, M.B. Johnston, L.M. Herz, H.J. Snaith, Energy Environ. Sci. 7 (2014) 982.

[15] N.G. Park, J. Phys. Chem. Lett. 4 (2013) 2423.

[16] Z.G. Xiao, Q.F. Dong, C. Bi, Y.C. Shao, Y.B. Yuan, J.S. Huang, Adv. Mater. 26 (2014) 6503.

[17] M. Kaltenbrunner, G. Adam, E.D. Głowacki, M. Drack, R. Schwödiauer, L. Leonat, D.H. Apaydin, H. Groiss, M.C. Scharber, M.S. White, N.S. Sariciftci, S. Bauer, Nat. Mater. 14 (2015) 1032.

[18] C. Bi, Y. Yuan , Y.J. Fang, J.S. Huang, Adv. Energy Mater. 5 (2015) 1401616.

[19] M. Cheng, B. Xu, C. Chen , X.C. Yang, F.G. Zhang, Q. Tan, Y. Hua, L. Kloo, L.C. Sun, Adv. Energy Mater. 5 (2015) 1401720.

[20] E.L. Unger, E.T. Hoke, C.D. Bailie, W.H. Nguyen, A.R. Bowring, T. Heumüller, M.G. Christoforo, M.D. McGehee, Energy Environ. Sci. 7 (2014) 3690.

[21] J.A. Christians, P.A.M. Herrera, P.V. Kamat, J. Am. Chem. Soc. 137 (2015) 1530.

[22] J. Kim, G. Kim, H. Back, J. Kong, I.W. Hwang, T.K. Kim, S. Kwon, J.H. Lee, J. Lee, K. Yu, C.L. Lee, H. Kang, K. Lee, Adv. Mater. 28 (2016) 3159.

[23] L.F. Liu, A. Mei, T.F. Liu, P. Jiang, Y.S. Sheng, L.J. Zhang, H.W. Han, J. Am. Chem. Soc. 137 (2015) 1790.

[24] Z.K. Wang, M. Li, Y.G. Yang, Y. Hu, H. Ma, X.Y. Gao, L.S. Liao, Adv. Mater. 28 (2016) 6695.

[25] H.C. Kwon, A. Kim, H. Lee, D. Lee, S. Jeong, J. Moon, Adv. Energy Mater. 6 (2016) 1601055.

[26] C. Roldán-Carmona, O. Malinkiewicz, R. Betancur, G. Longo, C. Momblona, F. Jaramillo, L. Camachob, H.J. Bolink, Energy Environ. Sci. 7 (2014) 2968.

[27] C.D. Bailie, M.G. Christoforo, J.P. Mailoa, A.R. Bowring, E.L. Unger, W.H. Nguyen, J. Burschka, N. Pellet, J.Z. Lee, M. Grätzel, R. Noufi, T. Buonassisi, A. Salleoa, M.D. McGehee, Energy Environ. Sci. 8 (2015) 956.

[28] C.T. Yip, H.T. Huang, L.M. Zhou, K.Y. Xie, Y. Wang, T.H. Feng, J. Li, W.Y. Tam, Adv. Mater. 23 (2011) 5624.

[29] X.N. Dang, J.F. Qi, M.T. Klug, P.Y. Chen, P.T. Hammond, A.M. Belcher D.S. Yun, N.X. Fang, Nano Lett. 13 (2013) 637.

[30] S. Chang, Q. Li, X.D. Xiao, K.Y. Wong, T. Chen, Energy Environ. Sci. 5 (2012) 9444.

[31] L. Zhou, X.Q. Yu, J. Zhu, Nano Lett. 14 (2014) 1093.

[32] N.Q. Fu, Y. Liu, Y.C. Liu, W. Lu, L.M. Zhou, F. Peng, H.T. Huang, J. Mater. Chem. A 3 (2015) 20366.

[33] L. Zhou, Y.L. Tan, D.X. Ji, B. Zhu, P. Zhang, J. Xu, Q.Q. Gan, Z.F. Yu, J. Zhu, Sci. Adv. 2 (2016) e1501227.

[34] M.Y. Tang, L. Zhou, S. Gu, W.D. Zhu, Y. Wang, J. Xu, Z.T. Deng, T. Yu, Z.D. Lu, J. Zhu, Appl. Phys. Lett. 109 (2016) 183901.

[35] S.W. Baek, G. Park, J. Noh, C. Cho, C.H. Lee, K. Seo, H. Song, J.Y. Lee, ACS Nano 8 (2014) 3302.

[36] C.H. Chou, F.C. Chen, Nanoscale 6 (2014) 8444.

[37] F.P.G. Arquer, A. Mihi, D. Kufer, G. Konstantatos, ACS Nano 7 (2013) 3581.

[38] Z.C. Yuan, Z.W. Wu, S. Bai, Z.H. Xia, W.D. Xu, T. Song, H.H. Wu, L.H. Xu, J.J. Si, Y.Z. Jin, B.Q. Sun, Adv. Energy Mater. 5 (2015) 1500038.

[39] C.T. Yip, X.L. Liu, Y.Y. Hou, W. Xie, J.J. He, S. Schlücker, D.Y. Lei, H.T. Huang, Nano Energy 26 (2016) 297.

[40] S.H. Liu, R.B. Jiang, P. You, X.Z. Zhu, J.F. Wang, F. Yan, Energy Environ. Sci. 9 (2016) 898.

[41] M. Saliba, W. Zhang, V.M. Burlakov, S.D. Stranks, Y. Sun, J.M. Ball, M.B. Johnston, A. Goriely, U. Wiesner, H.J. Snaith, Adv. Funct. Mater. 25 (2015) 5038.

[42] W. Zhang, M. Saliba, S.D. Stranks, Y. Sun, X. Shi, U. Wiesner, H.J. Snaith, Nano Lett. 13 (2013) 4505.

[43] J.B. Khurgin, G. Sun, R.A. Soref, Appl. Phys. Lett. 94 (2009) 071103.

[44] V. Myroshnychenko, J. Rodríguez-Fernández, I. Pastoriza-Santos, A.M. Funston, C. Novo, P. Mulvaney, L.M. Liz-Marzán, F.J.G. Abajo, Chem. Soc. Rev. 37 (2008) 1792.

[45] Y.J. Xiang, X.C. Wu, D.F. Liu, Z.Y. Li, W.G. Chu, L.L. Feng, K. Zhang, W.Y. Zhou, S.S. Xie, Langmuir 24 (2008) 3465.

[46] Z.Y. Bao, D.Y. Lei, R. Jiang, X. Liu, J. Dai, J.F. Wang, H.L.W. Chan, Y.H. Tsang, Nanoscale 6 (2014) 9063.

[47] R.B. Jiang, H.J. Chen, L. Shao, Q. Li, J.F. Wang, Adv. Mater. 24 (2012) OP200.

[48] M.F. Cardinal, B. Rodríguez-González, R.A. Alvarez-Puebla, J. Pérez-Juste, L.M. Liz-Marzán, J. Phys. Chem. C 114 (2010) 10417.

[49] O. Peña-Rodríguez, U. Pal, Nanoscale 3 (2011) 3609.

[50] A.K. Samal, L. Polavarapu, S. Rodal-Cedeira, L.M. Liz-Marzán, J. Pérez-Juste, I. Pastoriza-Santos, Langmuir 29 (2013) 15076.

[51] N.Q. Fu, C. Huang, Y. Liu, X. Li, W. Lu, L.M. Zhou, F. Peng, Y.C. Liu, H.T. Huang, ACS Appl. Mater. Interfaces 7 (2015) 19431.

[52] F. Giordano, A. Abate1, J.P.C. Baena, M. Saliba, T. Matsui, S.H. Im, S.M. Zakeeruddin, M.K. Nazeeruddin, A. Hagfeldt, M. Gräetzel, Nat. Commun. 7 (2016) 10379.

[53] C. Huang, N.Q. Fu, F. Liu, L. Jiang, X. Hao, H.T. Huang, Solar Energy Mater. & Solar Cells 145 (2016) 231.

[54] W. Li, W. Zhang, S.V. Reenen, R.J. Sutton, J. Fan, A.A. Haghighirad, M.B. Johnston, L. Wang, H.J. Snaith, Energy Environ. Sci. 9 (2016) 490.

[55] H.F. Zarick, A. Boulesbaa, A. A. Puretzky, E.M. Talbert, Z.R. DeBra, N. Soetan, D.B. Geoheganc, R. Bardhan, Nanoscale 9 (2017) 1475.

[56] H.S. Kim, N.G. Park, J. Phys. Chem. Lett. 5 (2014) 2927.

Vitae

Dr. Nianqing Fu received his Ph.D. degree from Institute of Chemistry, Chinese Academy of Science in 2013. He carried out his

research as a Research Associate in the Hong Kong Polytechnic University from 2013 to 2015. Currently, he is an associate professor in School of Materials and Engineering, South China University of Technology. His research interests mainly focus on the developing of semiconductor materials for photovoltaics, especially for dye-sensitized solar cells and perovskite solar cells.

Mr. Zhiyong Bao received his B.S. degree from HeFei Universitity of Technology in 2008. Now he is a Ph.D student at the department of Applied Physics, the Hong Kong Polytechnic University. His research interests include chiral plasmonics and plasmon-assisted photocatalysis.

Dr. Yong-Liang Zhang received his Ph.D degree from Chinese Academy of Science in 2008. He is currently a research fellow in the department of applied physics in the Hong Kong Polytechnic University. His current research focuses on the field of nanophotonics, including plasmonics, transformation optics and topological photonics.
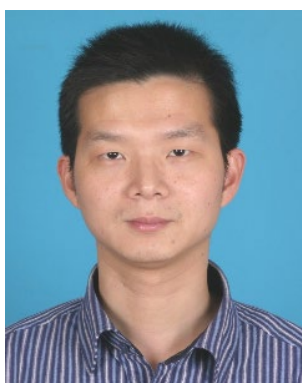
Dr. Guoge Zhang received his Ph.D. in Materials Science from Nanyang Technological University, Singapore in 2002. Since December 2008, he has been an associate professor in the School of Materials and Engineering, South China University of Technology. His research focuses on functional materials for energy conversion

and storage, such as supercapacitor.

Dr. Shanming Ke received his Ph.D degree in Materials Science from Northwestern Polytechnical University in 2008. He attended the Hong Kong Polytechnic University and worked as a Research Associate during 2008-2012. Currently, he is an associate professor of College of Materials Science and Engineering, Shenzhen University. His current research interests include ferroelectric materials, functional oxide thin film and perovskite solar cells.
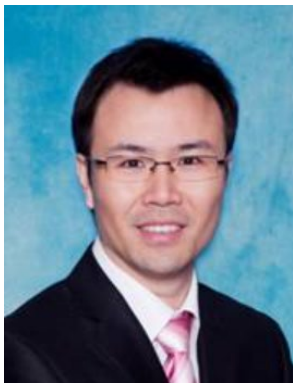
Dr. Peng Lin received his Ph.D. degree in physics from Hong Kong Polytechnic University in 2012. Now, he works in Shenzhen University (College of Materials Science and Engineering) as an associate professor. His research interests have been focused on biosensor, transistor, functional thin films for devices and organic solar cells.

Dr. J.Y. Dai is a Professor in Department of Applied Physics in the Hong Kong Polytechnic University. He obtained his Ph.D. degree from Chinese Academy of Sciences, Master degree from Tsinghua University and Bachelor degree from Fudan University. His research interests are nanomaterials fabrications and applications, functional

metal oxide thin films and device, medical ultrasound transducers and imaging
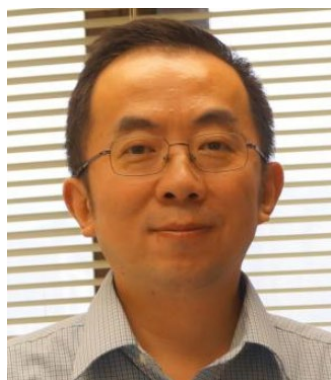
Dr. Haitao Huang received his Ph.D in Materials Science from Nanyang Technological University, Singapore in 2000. He is currently the Associate Professor in the Department of Applied Physics, the Hong Kong Polytechnic University. He has published over 190 refereed journal papers on energy materials (supercapacitors, lithium-ion batteries and solar cells) and ferroelectric materials. He obtained the "Outstanding Achievement Award" from the Asia Pacific Society for Materials Research in 2014. He is currently on the editorial board of *Scientific Reports* and *Composites Communications*, and the advisory board of *Journal of Materials Chemistry C*.
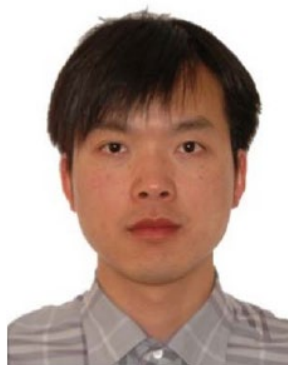
Dr. Dang Yuan Lei obtained his Ph.D. degree in Physics from Imperial College London in 2011 and his Ph.D. thesis was awarded the Imperial's prestigious prize "Anne Thorne Ph.D. Thesis Prize". Since September 2012, he has been an assistant professor with the Department of Applied Physics at The Hong Kong Polytechnic University. His current research centers on nanophotonics and nanomaterials studies,with particular interest in surface plasmon enhanced light-matter interaction at the nanoscale and their applications in energy harvesting, optoelectronic devices, biochemical sensing and biomedical imaging.